Bipolar charge-carrier injection in semiconductor/insulator/conductor heterostructures: self-consistent consideration

S.V. Yampolskii,[*] Yu.A. Genenko, C. Melzer, K. Stegmaier, and H. von Seggern

Institute of Materials Science, Darmstadt University of Technology,
Petersenstraße 23, D-64287 Darmstadt, Germany

(Dated: November 26, 2008)

A self-consistent model of bipolar charge-carrier injection and transport processes in a semiconductor/insulator/conductor system is developed which incorporates space-charge effects in the description of the injection process. The amount of charge-carriers injected is strongly determined by the energy barrier emerging at the contact, but at the same time the electrostatic potential generated by the injected charge-carriers modifies the height of this injection barrier itself. In our model, self-consistency is obtained by assuming continuity of the electric displacement and of the electrochemical potential all over the system. The constituents of the system are properly taken into account by means of their respective density of state distributions. The consequences resulting from our model are discussed on the basis of an indium tin oxide/organic semiconductor/conductor structure. The distributions of the charge carriers and the electric field through the electrodes and the organic layer are calculated. The recombination- and current-voltage characteristics are analyzed for different heights of injection barriers and varying values of the recombination rate and compared with the measured current-voltage dependences for an indium tin oxide/poly(phenylene vinylene)/Ca structure. The voltage dependences of the recombination efficiency for the different values of injection barriers and recombination rate reveal optimum conditions for the device performance.

PACS numbers: 73.40.Lq, 72.80.Le

I. INTRODUCTION

Though the problem of bipolar charge injection in insulator media is many years old[1,2,3,4], it anew became of great interest during last years in view of application of insulating materials as basic elements of electronic devices such as ferroelectric random access memories (FeRAMs)[5], organic field-effect transistors (OFETs) or organic light-emitting diodes (OLEDs)[6,7,8,9]. In the latter devices organic semiconductors are used which show many properties of dielectric materials, especially relatively large band gaps and thus, a low intrinsic charge carrier density. The charge carriers have to be injected into the organic layer from the electrodes and thereby must overcome the injection barriers at the organic/electrode interfaces. It is experimentally established that the injection conditions influence significantly the OLED performance[10,11,12,13].

Different models for the injection process are proposed in the literature. For low injection barriers, one expects the contact to be Ohmic, meaning that the contact is able to supply more charges per unit time than the bulk of the insulator can transport. In this case, a space-charge region is formed and the electric field at the interface is supposed to vanish[14]. Because excess charge-carriers dominate the charge transport in insulators, a space-charge-limited current (SCLC) density of the form $j \sim V^2/L^3$ is observed (in the absence of charge-carrier traps), where L is the sample thickness and V is the applied voltage. Current-voltage (IV) characteristics of space-charge limited devices are determined by the bulk properties of the insulator with no influence of the contact properties[15,16,17].

For high injection barriers, one anticipates the injection rate across the conductor/insulator interface to dominate the IV characteristic of the system. The models to describe injection are the Fowler-Nordheim (FN) tunneling model or the Richardson-Schottky (RS) model for thermionic injection[18]. The FN model assumes tunneling through a triangular barrier into an unbound continuum of states. The RS model on the other hand describes charge injection as a thermally activated hopping over the potential barrier, where barrier lowering due to the superposition of the external electrostatic potential and the image-charge potential is considered. An attempt to incorporate space-charge effects into the hopping injection model was undertaken in Refs. 19,20. However, all these models consider injection as a single electron process.

An alternative description of the injection process is given by the drift-diffusion theory involving electron-electron interaction in a mean-field approximation[7,21]. In this homogeneous continuum model widely used for the description of conventional crystalline semiconductors, the drift-diffusion equation in combination with the Poisson equation involves space-charge effects, but meets the problem of self-consistency in the boundary conditions. Namely, the electrostatic potential generated by the injected charge carriers modifies the injection barrier, but on the other hand the amount of charge-carriers injected per unit time depends on the barrier height. Thus, the values of the electrical field and charge-carrier density at the interface cannot be imposed but have to be found self-consistently implying the modification of the injection barrier, too. An effort to perform a self-consistent

analysis of the contact phenomena was made in Ref. 22. However, the current and the field in this approach were not defined in a self-consistent way. This can be performed if the drift-diffusion theory involves both, the insulator and the conductor side of the system, in analogy to a strongly asymmetric *pn*-junction. In the work of Neumann *et al.*[23], a self-consistent numerical treatment of the unipolar injection and transport processes in a conductor/insulator/conductor device was presented in which continuity of the electrochemical potential and the electric displacement was assumed everywhere in the system, in particular at the contacts. The conductor and the insulator were characterized by their specific density of state (DOS) distributions. The exact analytical solution in a self-consistent manner for the charge injection across the sole conductor/insulator interface has been also obtained[24].

This model does not yet allow for a self-consistent description of organic light emitting diodes, where bipolar transport takes place[7,9,25,26]. To do so, one has to account for the recombination of charge carriers (holes and electrons) which are usually present in the organic constituent of the heterostructure under consideration. In such systems the recombination is often believed to be of Langevin type[27,28], *i.e.* is considered as a bimolecular process. Many OLED models involve the recombination of electrons and holes (see, for example, Refs. 6,7,17,29,30,31,32,33,34). Probably, the most complete description was presented by Malliaras and Scott[35,36], who included a surface recombination at the contacts as well as a bimolecular recombination kinetics and diffusion in the bulk. However, the assumed boundary conditions for Ohmic contacts excluded diffusion at the contacts, where it is most important. A comprehensive one-dimensional numerical model accounting for space-charge effect was developed by Tutiš *et al.*[37] which comprised the hopping transport in single and bilayer devices and tunnel injection from electrodes. However, besides the injection barriers given by the bare difference of the chemical potential in the metal and the frontier molecular orbital in the organic material this model involves a range of artifacts such as tunneling factors, effective attempt frequencies, etc. Hence, in spite of a good agreement with experiments, this numerical tool is very complicated.

In the present paper, we apply the diode model given in Ref. 23 to elaborate a self-consistent OLED model. The properties of a semiconductor/organic/conductor structure are modeled where holes and electrons are simultaneously injected from an indium tin oxide (ITO) anode and a Ca cathode into the organic layer, respectively. The focus will be on the influence of the injection barriers and the recombination on the spatial distribution of the injected charge carriers and on the resulting *IV* characteristics as well as recombination efficiencies. Therefore, for simplicity, trap states and a field dependent mobility of the organic semiconductor constituent will be excluded at this stage.

The paper is organized as follows. In Sec. II we present the theoretical model of the charge injection in semiconductor/insulator/conductor structure. Then, using specific material parameters, we model the spatial distributions of the charge-carrier density and of the electric field (Sec. IIIA). In Sec. IIIB, the *IV* characteristics of the system (Sec. IIIB) are calculated varying the heights of injection barriers and the rate of the Langevin recombination. We also discuss the calculated voltage dependences of the recombination efficiency of the considered structure (Sec. IIIC). Our model is applied to a measured *IV* characteristic of an OLED composed of a poly(phenylene vinylene) (PPV) organic single layer sandwiched between ITO and Ca electrodes (Sec. IIID). Finally, in Sec. IV our results are summarized.

II. MODEL

Let us consider an insulator of thickness L sandwiched in between a semiconductor and a conductor electrode. The insulator is supposed to be extended over the space with $-L/2 \leq x \leq L/2$, whereas the semiconductor and conductor electrodes are extended over the half-spaces with $x < -L/2$ and $x > L/2$, respectively. We assume that the semiconductor electrode injects holes into the insulator layer while the conductor electrode injects electrons. The band structure of the system under consideration is shown schematically in Fig. 1.

A. Electrodes

Here we consider ITO as the hole-injecting electrode being an electron-conducting semiconductor with deep laying conduction band[21,38]. In the Thomas-Fermi approximation, one can deduce the electrochemical potential κ_s of the hole-injecting electrode as a function of the spatial coordinate x,

$$\kappa_s(x) = \frac{\hbar^2}{2m_s^*} \left[3\pi^2 n_s(x)\right]^{2/3} - e\phi(x), \qquad (1)$$

where $n_s(x)$ is the electron density in the electrode, m_s^* is the effective mass of the charge carriers in the semiconductor, $\hbar$ is Planck's constant, e is the elementary charge, and $\phi(x)$ is the electrostatic potential (notice that the energy level $E = 0$ coincides with the bottom of the semiconductor conduction band).

In general, everywhere in the heterostructure the electrochemical potential $\kappa(x)$ relates the steady-state current density j with the charge-carrier density. For a one-dimensional geometry, the current remains constant across the whole space and j is given by the conductivity σ and the derivative of $\kappa(x)$.

Accordingly, for the hole-injecting electrode,

$$j = \mu_s n_s(x) \frac{d\kappa_s(x)}{dx}, \qquad (2)$$

where μ_s is the charge-carrier mobility in the semiconducting electrode. The electric field $F_s(x)$ in the electrode obeys Gauss law,

$$F_s'(x) = -\frac{e}{\epsilon_s \epsilon_0} \delta n_s(x), \qquad (3)$$

where ϵ_s is the relative permittivity of the electrode, $\delta n_s(x) = n_s(x) - n_{\infty,s}$ is the excess electron density near the interface with respect to the electron density in the conduction band at infinite distance from the semiconductor/insulator interface, $n_{\infty,s}$. The value of this excess density is supposed to be small in comparison with the background electron density, $|\delta n_s(x)| \ll n_{s,\infty}$. Hence, the linearized Thomas-Fermi approximation can be applied, leading to a differential equation for F_s,

$$\frac{j}{\sigma_s} = -l_{TF,s}^2 F_s''(x) + F_s(x), \qquad (4)$$

with the conductivity in the electrode $\sigma_s = e\mu_s n_{\infty,s}$ and

$$l_{TF,s} = \sqrt{\frac{2}{3} \frac{\epsilon_s \epsilon_0 \kappa_{\infty,s}}{e^2 n_{\infty,s}}}, \qquad (5)$$

being the Thomas-Fermi screening length of the electrode. Here, $\kappa_{\infty,s}$ is the Fermi level of electrons with respect to the bottom of the conduction band.

Since the space-charge zone in the electrode is of finite thickness, the gradient of $F_s(x)$ has to vanish at infinite distance from the contact, and the solution for the electric field in the electrode reads

$$F_s(x) = \frac{j}{\sigma_s} + \left[F_s\left(-\frac{L}{2}\right) - \frac{j}{\sigma_s} \right] \exp\left(\frac{x + L/2}{l_{TF,s}} \right), \quad (6)$$

where the field in the electrode at the semiconductor/insulator interface, $F_s(-L/2)$, is unknown and has to be determined by the boundary conditions.

The distribution of the electric field in the electron-injecting electrode (conductor) is found in the same way as above. Even though this derivation was performed for a semiconductor it may be still meaningful for simple metals[39]. The electrochemical potential in the conductor reads

$$\kappa_c(x) = \frac{\hbar^2}{2m_c^*} \left[3\pi^2 n_c(x) \right]^{2/3} - e\phi(x) + E_b, \qquad (7)$$

where $n_c(x)$ is the electron density in the electrode, m_c^* is the effective mass in the conductor and E_b is the bottom of the conduction band. Performing calculations in the similar manner as for the hole-injecting electrode, we obtain the electric field in the conductor electrode,

$$F_c(x) = \frac{j}{\sigma_c} + \left[F_c\left(\frac{L}{2}\right) - \frac{j}{\sigma_c} \right] \exp\left(-\frac{x - L/2}{l_{TF,c}} \right), \quad (8)$$

with the unknown electric field $F_c(L/2)$ at the insulator/conductor interface again being determined by the boundary conditions, the conductivity $\sigma_c = e\mu_c n_{\infty,c}$ and the Thomas-Fermi screening length

$$l_{TF,c} = \sqrt{\frac{2}{3} \frac{\epsilon_c \epsilon_0 \kappa_{\infty,c}}{e^2 n_{\infty,c}}}. \qquad (9)$$

Here μ_c is the electron mobility of the metal electrode, $\kappa_{\infty,c}$ is the Fermi level of electrons with respect to the conduction band bottom, $n_{\infty,c}$ is the background electron density in the conduction band at infinite distance from the conductor/insulator interface and ϵ_c is the relative permittivity of the conductor.

B. Insulator

The energetic differences between the Fermi levels κ_∞ in the electrodes and the bottom of the conduction band or the top of the valence band in the insulator are defined as the injection barriers Δ_n and Δ_p for electrons and holes, respectively. These barriers relate to the difference between the electrode work functions E_A as well as to the insulator interband gap energy E_g:

$$E_{A,s} - \Delta_n^- = E_{A,c} - \Delta_n^+, \qquad (10)$$

$$\Delta_n^- + \Delta_p^- = \Delta_n^+ + \Delta_p^+ = E_g. \qquad (11)$$

From now on, the minus and plus superscripts denote the barriers at the interfaces $x = -L/2$ and $x = L/2$, respectively.

Let us characterize the insulator by the DOS functions, $g_{n,i}(E)$ and $g_{p,i}(E)$, describing extended states in the conduction and valence bands in which electron and hole transport takes place, respectively. Due to the large value of the energy gap, it is possible to introduce two separate electrochemical potentials; $\kappa_{n,i}$ for electrons and $\kappa_{p,i}$ for holes. Introducing band edges means that the DOS function $g_{n,i}(E) = 0$ when $E < 0$ and the DOS function $g_{p,i}(E) = 0$ when $E > 0$. Hence, the densities of electrons and holes in the extended states can be calculated using Boltzmann statistics, thus allowing solely for a proper description of non-degenerate insulators,

$$n_i(x) = \int_{-\infty}^{\infty} g_{n,i}\left[E - \Delta_n^- - \kappa_{\infty,s} + e\phi(x) \right] f_n(E)\, dE, \tag{12}$$

$$p_i(x) = \int_{-\infty}^{\infty} g_{p,i}\left[E + \Delta_p^- - \kappa_{\infty,s} + e\phi(x) \right] f_p(E)\, dE, \tag{13}$$

$$f_n(E) = \exp\left[\frac{\kappa_{n,i}(x) - E}{kT} \right], \qquad (14)$$

$$f_p(E) = \exp\left[\frac{E - \kappa_{p,i}(x)}{kT}\right], \qquad (15)$$

here T is the absolute temperature and k is the Boltzmann constant.

The electrochemical potentials $\kappa_{n,i}$ and $\kappa_{p,i}$ are consequently expressed in terms of the charge-carrier densities n_i and p_i,

$$\kappa_{n,i}(x) = kT\ln\left[\frac{n_i(x)}{N}\right] + \Delta_n^- + \kappa_{\infty,s} - e\phi(x), \quad (16)$$

$$\kappa_{p,i}(x) = -kT\ln\left[\frac{p_i(x)}{P}\right] - \Delta_p^- + \kappa_{\infty,s} - e\phi(x), \quad (17)$$

where the quantities

$$N = \int_0^\infty g_n(E')\exp\left(-\frac{E'}{kT}\right)dE', \qquad (18)$$

and

$$P = \int_{-\infty}^0 g_p(E')\exp\left(\frac{E'}{kT}\right)dE' \qquad (19)$$

can be understood as the effective total densities of states available in the conduction and valence bands of the insulator, respectively.

The total current density in the insulator consists of the electron and hole contributions and reads:

$$j = j_p(x) + j_n(x), \qquad (20)$$

with

$$j_n = \sigma_{n,i}(x)F_i(x) + kT\mu_{n,i}n_i'(x), \qquad (21)$$
$$j_p = \sigma_{p,i}(x)F_i(x) - kT\mu_{p,i}p_i'(x), \qquad (22)$$

where $\sigma_{n,i} = e\mu_{n,i}n(x)$ and $\sigma_{p,i} = e\mu_{p,i}p(x)$ are the conductivities of electrons and holes, respectively, with the respective electron and hole mobilities $\mu_{n,i}$ and $\mu_{p,i}$. When accounting for the electron-hole recombination in the insulator, the steady-state continuity equations for holes and electrons read

$$\frac{dj_n(x)}{dx} = eBR\left[n_i(x)p_i(x) - n_{\text{int}}^2\right], \qquad (23)$$

$$\frac{dj_p(x)}{dx} = -eBR\left[n_i(x)p_i(x) - n_{\text{int}}^2\right], \qquad (24)$$

where $0 \leq R \leq 1$ is the recombination parameter, B is the Langevin recombination coefficient,

$$B = \frac{e}{\epsilon_i\epsilon_0}(\mu_{n,i} + \mu_{p,i}), \qquad (25)$$

and the intrinsic charge density n_{int} is given by $n_{\text{int}}^2 = NP\exp(-E_g/kT)$[18,33]. We note one more time that, in steady state, the total current remains constant through the entire system.

Finally, from Eqs. (21)-(24) we obtain the system of equations for the charge-carrier densities and the electric field, governed by Gauss law, in the insulator:

$$n_i'(x)F_i(x) + n_i(x)F_i'(x) + \frac{kT}{e}n_i''(x)$$
$$= \frac{B}{\mu_{n,i}}R\left[n_i(x)p_i(x) - n_{\text{int}}^2\right], \qquad (26)$$

$$p_i'(x)F_i(x) + p_i(x)F_i'(x) - \frac{kT}{e}p_i''(x)$$
$$= -\frac{B}{\mu_{p,i}}R\left[n_i(x)p_i(x) - n_{\text{int}}^2\right], \qquad (27)$$

$$F_i'(x) = \frac{e}{\epsilon_i\epsilon_0}[p_i(x) - n_i(x)]. \qquad (28)$$

C. Self-consistency and boundary conditions at the contacts

Assuming no dipole layer or surface charge at the interfaces one has to require continuity of the electrical displacement and of the electrochemical potential[40],

$$\epsilon F(x) = \text{continuous}, \qquad (29)$$
$$\kappa(x) = \text{continuous}. \qquad (30)$$

This continuity may be provided self-consistently matching the expressions of the electrical displacements and electrochemical potentials. In particular, one can write

$$\epsilon_s F_s\left(-\frac{L}{2}\right) = \epsilon_i F_i\left(-\frac{L}{2}\right), \quad \epsilon_i F_i\left(\frac{L}{2}\right) = \epsilon_c F_c\left(\frac{L}{2}\right). \qquad (31)$$

Matching the electrochemical potentials we obtain four nonlinear boundary conditions:

$$\ln\left[\frac{n_i(-L/2)}{N}\right] + \frac{\Delta_n^-}{kT} + \frac{el_{TF,s}}{kT}\left[\frac{\epsilon_i}{\epsilon_s}F_i\left(-\frac{L}{2}\right) - \frac{j}{\sigma_s}\right] = 0, \qquad (32)$$

$$\ln\left[\frac{p_i(-L/2)}{P}\right] + \frac{\Delta_p^-}{kT} - \frac{el_{TF,s}}{kT}\left[\frac{\epsilon_i}{\epsilon_s}F_i\left(-\frac{L}{2}\right) - \frac{j}{\sigma_s}\right] = 0, \qquad (33)$$

$$\ln\left[\frac{n_i(L/2)}{N}\right] + \frac{\Delta_n^+}{kT} - \frac{el_{TF,c}}{kT}\left[\frac{\epsilon_i}{\epsilon_c}F_i\left(\frac{L}{2}\right) - \frac{j}{\sigma_c}\right] = 0, \qquad (34)$$

$$\ln\left[\frac{p_i(L/2)}{P}\right] + \frac{\Delta_p^+}{kT} + \frac{el_{TF,c}}{kT}\left[\frac{\epsilon_i}{\epsilon_c}F_i\left(\frac{L}{2}\right) - \frac{j}{\sigma_c}\right] = 0, \qquad (35)$$

which depend on parameters of both the insulator and the electrodes. Notice, that from Eqs. (32) and (35) the following relations are obtained:

$$n_i\left(-L/2\right)p_i\left(-L/2\right) = n_i\left(L/2\right)p_i\left(L/2\right)$$
$$= NP\exp\left(-\frac{E_g}{kT}\right). \qquad (36)$$

As the last boundary condition, we can use the value of the current density taken at one of the interfaces:

$$j = j_p\left(-L/2\right) + j_n\left(-L/2\right). \qquad (37)$$

III. PHYSICAL AND NUMERICAL ANALYSIS

The full set of nonlinear differential equations (26)-(28) with the nonlinear boundary conditions (32)-(35) and (37) has to be solved numerically.

As an example for an insulator, an organic semiconductor can be considered, exhibiting many typical characteristics of insulators such as relatively large band gaps up to 3 eV and, hence, the absence of intrinsic charge carriers. In simple organic light-emitting diodes (OLEDs) a thin layer of a organic semiconductor is contacted with a low work-function metal and a high work-function transparent conducting oxide. Here, we consider indium tin oxide (ITO) as the hole-injecting electrode and Ca as the electron-injecting contact. ITO is typically employed as anode in OLEDs, since it provides a decent conductivity and a sufficient high work function (up to 5 eV) to allow for efficient hole injection while being transparent in the visible region of the light spectrum to ensure light out-coupling. On the other hand, Ca with a work function of about 2.9 eV delivers efficiently electrons and, hence, is used as cathode in OLEDs. From now on, it is assumed that the material specific quantities of the organic semiconductor and the electrodes adopt the typical values given in Table I.

The injection barriers $\Delta_{p,n}$ are given by the energetic difference between the highest occupied molecular orbital (HOMO) or the lowest unoccupied molecular orbital (LUMO) in the organic semiconductor and κ_∞ of the respective electrodes. Change of the barrier heights at the interfaces and of the gap energy in the organic semiconductor, leaving the electrodes unchanged, can be understood as considering different organic semiconductors. Here, for simplicity and without loss of generality, we assume that the gap energy in organic constituent is fixed. Therefore, changing the value of the barrier height at one interface results in equally shifted energies of the HOMO and LUMO levels which entails the change of the barrier at another interface.

Notice, that specifying the material parameters for the insulator and the electrodes leads to substantial consequences for the boundary conditions. The current density j is multiplied by the small factors $l_{TF,s}/kT\mu_s n_{\infty,s}$ in Eqs. (32)-(33) and by the small factor $l_{TF,c}/kT\mu_c n_{\infty,c}$

in Eqs. (34)-(35). Hence, the boundary conditions do not depend directly on j in most practical cases. Under this approximation, equations (33)-(34) can be reduced to

$$p_i\left(-\frac{L}{2}\right) = P\exp\left[-\frac{\Delta_p^-}{kT} + \frac{el_{TF,s}}{kT}\frac{\epsilon_i}{\epsilon_s}F_i\left(-\frac{L}{2}\right)\right], \quad (38)$$

$$n_i\left(\frac{L}{2}\right) = N\exp\left[-\frac{\Delta_n^+}{kT} + \frac{el_{TF,c}}{kT}\frac{\epsilon_i}{\epsilon_c}F_i\left(\frac{L}{2}\right)\right]. \quad (39)$$

As a consequence, the dependence of $F_i(\mp L/2)$ as well as $p_i(-L/2)$ or $n_i(L/2)$ on the current is only due to Eq. (37). Apparently, the injection barriers effectively vary with $\propto F_i(\mp L/2)$ similarly to the case of unipolar carrier injection[23,24]. This change in injection barriers leads to the definition of effective injection barriers,

$$\Delta_{\text{eff}}^- = \Delta_p^- - e\frac{\epsilon_i}{\epsilon_s}F_i\left(-\frac{L}{2}\right)l_{TF,s} \qquad (40)$$

$$= \Delta_p^- - eF_s\left(-\frac{L}{2}\right)l_{TF,s}, \qquad (41)$$

$$\Delta_{\text{eff}}^+ = \Delta_n^+ - e\frac{\epsilon_i}{\epsilon_c}F_i\left(\frac{L}{2}\right)l_{TF,c} \qquad (42)$$

$$= \Delta_n^+ - eF_c\left(\frac{L}{2}\right)l_{TF,c}. \qquad (43)$$

The changes in the effective injection barriers correspond to the amount of energy a charge carrier gains (or loses) in the electric field prevailing in the electrodes. This change, as is seen from Eqs. (41) and (43), is not necessarily negative but can be positive, since a space-charge region at the interface might serve as a potential barrier itself. The electric field, however, cannot be arbitrary large. Assuming Boltzmann statistics for both injected electrons and holes requires that the electrochemical potentials (16) and (17) do not approach the respective band edges so that inequalities $n_i \ll N$ ans $p_i \ll P$ hold. Considering boundary conditions (38)-(39), this imposes a requirement on the electric field at the interfaces so that both effective barriers (40) and (42) remain positive. To keep the validity of Boltzmann statistics the above requirements are controlled during the further numerical calculations.

A. Spatial distributions of charge carriers and electric field

First, we calculate the spatial distributions of charge carriers and the electric field in the organic layer without accounting for recombination ($R = 0$). The barrier height for hole injection was varied from 0 to 0.57 eV. For the parameters from Table I, using equations (10)-(11) and due to the fixed gap energy of 2.4 eV a hole injection barrier of 0.57 eV at the anode corresponds to a barrier-free electron injection from the opposite electrode. In Fig. 2 the distributions of holes and electrons

TABLE I: Typical material parameters for electrodes and an organic semiconductor (Refs. 21,41,42,43,44). The parameters are deduced assuming $T = 300$ K and m_e is the free electron mass.

	ITO							Organic semiconductor					Ca				
$l_{TF,s}$	$n_{\infty,s}$	ϵ_s	μ_s	m_s^*	$\kappa_{\infty,s}$	$E_{A,s}$	N,P	ϵ_i	$\mu_{p,i}$	$\mu_{n,i}$	E_g	$l_{TF,c}$	$n_{\infty,c}$	μ_c	$\kappa_{\infty,c}$	$E_{A,c}$
(Å)	(cm^{-3})		$\left(\dfrac{\text{cm}^2}{\text{V s}}\right)$	(m_e)	(eV)	(eV)	(cm^{-3})		$\left(\dfrac{\text{cm}^2}{\text{V s}}\right)$	$\left(\dfrac{\text{cm}^2}{\text{V s}}\right)$	(eV)	(Å)	(cm^{-3})	$\left(\dfrac{\text{cm}^2}{\text{V s}}\right)$	(eV)	(eV)
8.6	10^{20}	9.3	30	0.35	0.225	4.7	10^{21}	3	10^{-4}	10^{-6}	2.4	0.8	$2.6\cdot10^{22}$	66.7	4.68	2.87

in the organic layer are depicted for two different current densities of $j = 2$ and 100 mA/cm^2. The electron and hole density profiles change slightly with the current but depend strongly on the respective injection barrier heights. When one injection barrier is small, a high charge carrier density appears near the respective electrode decreasing monotonously through the organic layer and dropping quickly near its ejecting electrode. In this case the injection barrier at the other contact is large and thus, the density of the respective charge carriers is relatively small. Due to the absence of recombination all injected charge carriers have to traverse the entire organic layer. The large amount of space charge emerging at the low injection-barrier electrode prevent the ejection of the traversed charge carriers injected at the high barrier contact. This gives rise to a local maxima of their concentration near their ejecting electrode. The effect is specific as long as no hole-electron recombination occurs.

The distribution of the electric field across the organic layer is shown in Fig. 3 for the same parameter values as in Fig. 2. The electric field strongly varies with the change of the injection barrier. When the heights of the injection barriers at the contacts differ significantly, one kind of the charge-carrier dominates. As a result, the electric field changes monotonously between the electrodes, just like in the single-interface case (see, for example, Ref. 24). In the limit of barrier-free injection the field profile beyond the virtual electrode[24] is well described in the frame of the space-charge approximation. Once the heights of electron and hole injection barriers at the cathode and the anode are comparable, nearly equal hole and electron densities prevail in the organic layer. Hence, the charge density is small and the electric field appears to be almost constant with a small maximum in the middle of the organic layer.

Charge recombination gives rise to severe changes in the charge carrier density and field distributions in the organic layer. First, let us consider the case of comparable injection barriers, *i.e.* $\Delta_p^- = 0.3$ eV and $\Delta_n^+ = 0.27$ eV. The dependences of charge-carrier densities on coordinate x are shown in Figs. 4,a and b for different values of the recombination parameter R. The annihilation of traversing holes with traversing electrons leads to a strong spatial decrease in the charge-carrier densities. The change occurs already for a small increase of the re-

combination parameter up to $R = 0.1$. A subsequent increase of the recombination parameter up to 1 influences the picture insignificantly. In Fig. 4,c the space distribution of the recombination rate Rn_ip_i is shown. To illustrate the position of the recombination zone, which is proportional to the product n_ip_i, the distribution of n_ip_i normalized by its maximum value is shown in Fig. 4,d. For small R the recombination zone extends almost over the entire organic layer, but with increase of R it moves close to the electron-injecting electrode. This is because of the assumed large difference (two orders of the magnitude) in the mobilities of the holes and electrons in the organic material. The injected holes can traverse nearly the entire organic layer before they recombine with the electrons. The influence of recombination on the respective electric field distribution is displayed in Fig. 5. Even small values of recombination parameter (up to $R = 0.1$) change the electric field significantly, moving its maximum to the region of the maximum of the recombination rate. At low R the charge density in the center of the device is small giving rise to a nearly constant electric field. At the contacts however, where one charge carrier specie dominates space-charge effects emerge. Upon increased R nearly the entire organic layer is dominated by holes and only close to the cathode a substantial electron density emerges. Hence, space-charge effects are important in the entire device.

In the case of strongly different injection barriers their influence becomes more pronounced. This is illustrated in Figs. 6 and 7, where the recombination zone and the distribution of electric field are shown for the barrier heights of $\Delta_p^- = 0.4$ eV and $\Delta_p^- = 0.2$ eV, respectively.

For $\Delta_p^- = 0.4$ eV the electric field distribution is dominated by the buildup of negative space charge. Due to the high hole mobility injected holes traverse the organic layer and recombine close to the cathode where the maximum electron density prevails. This holds for all R and thus, the recombination maximum is situated close to the cathode. For $\Delta_p^- = 0.2$ eV, when the injection of holes is more efficient than the injection of electrons, the field distribution is dominated by the buildup of positive space-charge. For very small R the maximum of recombination zone is situated near the hole-injecting electrode since the injected electrons can traverse the whole organic semiconductor without recombining and their density is

still locally increased near the hole-injecting electrode. However, with increased R the recombination probability increases and the few injected electrons recombine instantaneously after injection since their recombination rate exceeds their transport rate. Hence, the maximum of the $n_i p_i$ product moves to the cathode with increased R.

B. Current-voltage characteristics

Next, we calculate the current-voltage characteristics of the system under consideration. Knowledge about the distribution of the electric field gives access to the voltage drop V across the system for a given current density j and hence, to its IV characteristics.

The voltage drop at the device is defined as

$$V = \int_{-\infty}^{+\infty} F_d(x)\,dx - V_{bi}, \qquad (44)$$

where

$$F_d(x) = \begin{cases} F_s(x) - j/\sigma_s, & x < -L/2, \\ F_i(x), & -L/2 \le x \le L/2, \\ F_c(x) - j/\sigma_c, & x > L/2, \end{cases} \qquad (45)$$

and $-V_{bi}$ is the voltage drop in the case of $j = 0$, i.e. the built-in potential. Using the system of equations (26)-(28) and boundary conditions (32)-(35), the built-in potential can be obtained analytically. This calculation is presented in the Appendix. Similarly to the case of unipolar charge-carrier transport, the built-in potential is given by the difference of the electrode's work functions,

$$eV_{bi} = E_{A,c} - E_{A,s}. \qquad (46)$$

Integrating the field F_d, we obtain

$$\int_{-\infty}^{+\infty} F_d(x)\,dx = l_{TF,s}\left[\frac{\epsilon_i}{\epsilon_s}F_i\left(-\frac{L}{2}\right) - \frac{j}{\sigma_s}\right] + l_{TF,c}\left[\frac{\epsilon_i}{\epsilon_c}F_i\left(\frac{L}{2}\right) - \frac{j}{\sigma_c}\right] + \int_{-L/2}^{L/2} F_i(x)\,dx. \qquad (47)$$

Using the boundary conditions, the voltage may be rewritten in the shorter form

$$V = \frac{kT}{e}\ln\left[\frac{p_i(-L/2)}{p_i(L/2)}\right] + \int_{-L/2}^{L/2} F_i(x)\,dx. \qquad (48)$$

In Fig. 8 the resulting IV characteristics are presented for the case of absence of recombination when the barrier height Δ_p^- changes from 0 to 0.57 eV. At voltages $V \lesssim -V_{bi}$ there is no Ohmic-like $j \sim V$ behavior which has been obtained in the cases of the unipolar transport[23] or of the bipolar charge injection from Ohmic contacts[17]. In the calculated range of voltages (and currents) all IV characteristics exhibit only a tendency to this behavior. Hence, it can be supposed that the Ohmic region lies at even lower voltages. Near the built-in voltage, $-V_{bi}$, a relatively wide region starts where, for the cases of barrier-free injection of carriers (holes or electrons), the SCLC behavior $j \sim V^2$ of IV characteristics occurs. This behavior is similar to that described in the diffusion-free analysis in Ref. 45 and stems from the dominance of electrons or holes, respectively. When nonzero injection barriers exist for both kinds of charge carriers, the IV dependences differ from the SCLC behavior but all corresponding curves lie between the curves with $\Delta_p^- = 0$ and $\Delta_p^- = 0.57$ eV. For high voltages at all Δ_p^- the IV dependences tend to a transition in the $j \sim V^3$ regime which is intrinsic for systems with bipolar transport in the recombination-free case[17]. Yet, in the framework of our model this region can not be reached at some barrier

heights because the used Boltzmann statistics of carriers in the organic constituent is violated here.

When recombination is accounted for, the IV characteristics change substantially. This influence is demonstrated in Fig. 9 on the example of characteristics for the barrier heights of $\Delta_p^- = 0.3$ and 0.4 eV. One can see that the most significant effect occurs in the high-voltage part of the characteristics where the transition from the $j \sim V^3$ regime to the SCLC-like $j \sim V^2$ behavior occurs even for the smallest value of $R = 0.001$. At the same time, the remaining part of the IV characteristics virtually is not changed by the recombination. However, it should be noted that with increase of R the current density slightly increases in the low voltage part of the IV characteristics whereas in the region of the SCLC-like behavior a slight decrease of j is visible.

The significant change of the IV characteristics at high voltages can be related to the influence of the recombination on the modification of the injection barriers. The corresponding dependences of the effective barriers $\Delta_{\text{eff}}^{\pm}$ on the applied voltage V are presented in Fig. 10. In general, the effective barriers decrease with the voltage tending to become equal at vanishing barrier for the recombination-free case. However, recombination weakens this decrease so that nonzero effective barriers are obtained at much higher voltages. By that the difference between Δ_{eff}^- and Δ_{eff}^+ remains considerable and even increases significantly for high magnitudes of the recombination rate. Paradoxically, the prevailing injection bar-

riers provide a *significant* extension of the voltage range where the SCLC-like behavior of the *IV* characteristic occurs.

C. Recombination current and efficiency

Integrating the product $eBR\left[n_i\left(x\right)p_i\left(x\right)-n_{\mathrm{int}}^2\right]$ [*i.e.* the right-hand side of Eq. (23)] over the thickness of the organic layer, we obtain a quantity having the dimension of a current density and usually called the recombination current density, j_r (Ref. 7). It stands for the total number of recombination events in the volume of organic constituent per unit square of the interface, per unit time. This quantity determines the recombination efficiency of the device, $\eta_r = j_r/j$ (Ref. 7). The calculated dependences of the recombination current density on the applied voltage are given in Fig. 11 for the barrier heights $\Delta_p^- = 0.3$ and 0.4 eV. The total recombination current increases with increased recombination parameter R and thus a higher luminance of the OLED is expected. It is clearly seen from Fig. 11 that already for the smallest calculated values of the recombination parameter R a substantial recombination current is observed while in the range from $R = 0.1$ to 1 the increase in j_r rather weak.

In general, the recombination currents follow the *IV* characteristics with an increased total recombination rate for an increased current density. However, the dependence of the recombination efficiency η_r on the applied voltage unveil important details. In Fig. 12 the recombination efficiency is depicted using the same parameters as for the system in Fig. 11. The recombination efficiency shows features which have not been discussed in previous works [7,29,33,34,35,36] where different boundary conditions at the injecting interfaces have been assumed. In general, a maximum in $\eta_r\left(V\right)$ is found close to $-V_{bi}$ no matter which injection barriers have been considered. This may be explained by the detailed analysis of the carrier densities and partial currents as follows: a fast increase of the electric current j occurs at voltages $V \lesssim -V_{bi}$ (Ref. 23) corresponding to the Shockley diode equation for unipolar injection[18]. Assuming a virtually independent unipolar injection for electrons and holes from the two electrodes one can expect the faster increase of the recombination current j_r quadratic in carrier densities which results in the peak close to $-V_{bi}$. At higher bias $\eta_r\left(V\right)$ depends strongly on the injection barrier heights and the charge carrier mobilities. For rather balanced but high injection barriers ($\Delta_p^- = 0.3$ eV) there is a large range of voltage where the efficiency is strongly attenuated independently of the recombination parameter. Assuming that the built up of space-charge is small due to the substantial injection barriers, the electric field is constant in the device and the injection barrier lowering scales linearly with the applied voltage as can be seen from Fig. 10,a in between 3 and 30 V. However, for low bias the injection barrier lowering is negligible so that the

density of electrons and holes stays roughly constant for a wide voltage range. Therefore the recombination current does not change if the bias increases. At the same time, since the total current is proportional to the electric field a drop of the efficiency upon the bias increase is expected. For an initiation of barrier lowering, the charge carrier densities of electrons and holes grow exponentially with the barrier lowering and thus an increase in the recombination current sets in. The efficiency saturates and increases again. For a further increase in bias the reduction of the injection barrier heights is weakened since space charges emerge. The respective injection barriers tend to diverge leading to a higher injection barrier for holes than for electrons balancing the charge carrier densities in the insulator. Since balanced charge-carrier densities result in an optimized recombination rate the self-balancing effect leads to an increase in efficiency.

Introducing asymmetric injection barriers the efficiency-voltage characteristic changes dramatically. For a higher value of the hole injection barrier, $\Delta_p^- = 0.4$ eV, and thus a low electron injection barrier the attenuation of the efficiency due to high injection barriers is missing. The most pronounced change in the efficiency curve is the appearance of the peak denoted by D in Fig. 12,b for $R = 1$. Increasing the voltage coming from $-V_{bi}$ leads to a buildup of space-charge for the charge carriers with the lower barrier, in this case electrons. Strong injection of electrons contributes to the electric current j but does not add much to the recombination current because the minority carriers remain in the barrier-limited regime. This provides the fall of the efficiency down to the point C. However, since the electron mobility is low, the negative space charge does not result in a strong current. On the other hand, the Langevin recombination parameter B is large since it is dominated by the larger hole mobility. Therefore, the efficiency is not fully attenuated. In the area C to D where the electrons are already in the space-charge regime with approximately constant and low barrier, the barrier for holes decreases (see Fig. 10,b) providing exponential increase of the minority carriers. This does not contribute much to the electric current j but strongly promotes the recombination current j_r. Further increase of the voltage depresses the injection barrier at the hole-injecting side leading to an substantial amount of holes accumulated at the anode. Now the above mentioned self-balancing effect sets in and the efficiency tends to increase again. Apparently, the charge carrier mobilities are important for the efficiency peak D. Assuming comparable charge carrier mobilities for electrons and holes, a strong reduction of the efficiency can be observed below 30 V.

It should be also noted that the change of the mobility ratio (for example, by decrease of the hole mobility) not only varies quantitatively the values of the current and the efficiency but also acts strongly on the position and the shape of the recombination zone. This is seen from Fig. 13, where the spatial distributions of this zone,

calculated in several points of the $\eta_r(V)$ dependences of Fig. 12,b for the cases $\mu_{p,i} = \mu_{n,i}$ and $\mu_{p,i} = 100\ \mu_{n,i}$, are presented. With increased applied voltage, the recombination zone extends through the whole organic layer as long as equal mobilities $\mu_{p,i} = \mu_{n,i}$ are assumed, whereas in the case of the large mobility difference there is a pronounced peak of the recombination zone moving to the electron-injecting electrode since the injected holes are faster than the electrons.

Thus, additionally to the case of fully balanced injection and transport properties, which is often difficult to achieve in single-layer devices[7], it may be possible to maximize the recombination efficiency in an OLED with imbalanced injection and transport properties compensating the small amount of the minority carriers by their relatively high mobility with respect to the mobility of the dominating carriers.

D. Comparison with experiment

To evaluate the presented model it is compared to experimental data obtained from a diode consisting of a single poly(phenylene vinylene) (PPV) layer of thickness $L = 100$ nm sandwiched between ITO and Ca electrodes. The characteristic energies of the LUMO and HOMO levels of the employed PPV are 2.8 eV and 5 eV, respectively and the hole mobility $\mu_{p,i}$ equals $5 \cdot 10^{-7}$ cm^2/(V s) (Refs. 6,32). The ratio of the electron and hole mobilities is assumed to be $\mu_{n,i}/\mu_{p,i} = 0.01$. It is known, that the work function of ITO is sensitive to the cleaning procedure and thus, it may be varied from 4.7 eV to 5 eV (up to the energy of the HOMO level). Therefore, we are allowed to consider the injection barrier Δ_p^- as one of the fitting parameters. The other barrier, Δ_n^+, is supposed to be unchanged and equals 0.07 eV.

In Fig. 14 the measured IV characteristic of the ITO/PPV/Ca structure is shown as well as the IV dependences calculated for $\Delta_p^- = 0.1$ eV (the best fitting value) and for different values of fitting parameters R and $N(= P)$. On the one hand, the calculation satisfactory reproduces the magnitude and the general form of IV characteristic using reasonable parameters. On the other hand, however, the *exact* shape of the IV curve can not be fully approximated by a unique set of parameters. This is due to the fact that the proposed model misses still some important features of insulators, in particular of organic semiconductors. First of all, realistic DOS shapes for the LUMO and HOMO levels as well as trap levels in the insulator layer have to be accounted for. This leads effectively to a field and charge carrier density dependence of the mobilities which may increase the calculated currents at larger voltages. It should be also noted, that due to this the ratio of the hole and electron mobilities varies with the change of the applied voltage[6,32].

Comparing the luminance efficiency in Fig. 15 with the calculated recombination efficiency a good reproduction of the voltage dependence can be obtained above 3 V. Here, the calculated recombination efficiency was normalized to the measured luminance efficiency ignoring e.g. the voltage dependence of the extraction efficiency. There is, however, a strong discrepance of the measured and fitted efficiency curves at lower voltages. Again, this difference may be due to the absence of trap levels in our simple model. At low voltages, strong trapping could arise close to the electrode shifting the recombination zone to the injecting contact giving rise to a strong reduction of the luminance efficiency due to quenching effects[6,30,32].

Concentrating on the effect of injection on the device performance one has to consider also a possible formation of the dipole layers at the electrode/organic interface which may have crucial consequences for the prevailing charge-carrier injection barriers. Dipole layers may be a result of self-organization or a consequence of the deposition of some functional layer at the interface[46,47]. The phenomenon of a dipole-layer formation cannot be incorporated self-consistently in the developed phenomenological approach, however, an effective change in the injection barrier heights can be assumed. Notice, that in this case the magnitudes of injection barriers Δ_p^- and Δ_n^+ are decoupled and become independent.

If compared to other models of bipolar transport and recombination in OLEDs the model presented here describes satisfactorily a crossover from the high-voltage, space-charge limited regime to the low-voltage, barrier-dominated regime. Even the regime around the built-in potential which is problematic in theories using other boundary conditions[21,32,48] is well described. Comparing with very comprehensive discrete one-dimensional simulations by Tutiš *et al.*[37] our approach presents a simpler continuous description using a strongly reduced number of fitting parameters.

IV. CONCLUSIONS

In the calculation of the charge-carrier transport through insulators, the fundamental question about boundary conditions generally arises when charge-carrier injecting interfaces are involved. In this paper, a simple one-dimensional model describing the bipolar charge-carrier transport across a semiconductor/insulator/conductor structure was presented, where the problem of injection was for the first time solved self-consistently. Essentially, continuity of the electric displacement and the electrochemical potential was assumed, thus matching them at the injecting interfaces of the electrodes with the insulator. Additional boundary conditions were defined far into the electrode materials, where the influence of the involved materials on each other is negligible so that they can be regarded as independent. Considering the Poisson equation, the electric-field distributions and the current-voltage characteristics were derived using as an example the organic semicon-

ductor sandwiched between ITO and Ca electrodes. The influence of different injection conditions and recombination rates on the current transport properties of such a structure was analyzed. It was found that the injection barriers determine the dominating carrier type and strongly influence the distributions of the charge and of the induced field in the organic layer. The recombination influences on these quantities most strongly when the heights of injection barriers for holes and electrons are comparable. It was shown that the injection barriers and recombination together with the mobility ratio define the position and shape of the recombination zone in the organic layer as well as drastically affect the current-voltage characteristics of the considered diode structure. We have also found that in the case of significantly different injection barriers a high recombination efficiency of a diode may be still achieved in the case of a relatively high mobility of the minority carriers. Notice, that the controlling of the carrier mobility in organic devices is experimentally possible[49].

Finally, we can conclude that the presented self-consistent model of charge injection reveals unambiguously that injection barriers and recombination rate are the governing factors controlling the transport properties of semiconductor/insulator/conductor structures. On the other hand, this model cannot yet provide a complete description of the particular case of OLEDs because some specific features of these systems are still missing. Most important of them are the realistic DOS shapes including energetically distributed trap states[14,30,31,32] or concentration- and field-dependent carrier mobilities[50] characteristic of organic semiconductors. The latter feature is followed by the exponential-type dependence of the injection current on the device thickness[36,51] which can hardly be expected within our consideration. Further extension of the model concerning the inclusion of

the above-mentioned features is necessary for better application to experimental data and is now in preparation.

APPENDIX: CALCULATION OF THE BUILT-IN POTENTIAL IN THE CASE OF BIPOLAR TRANSPORT

The built-in potential defines as

$$V_{bi} = \int_{-\infty}^{+\infty} F_d(x)|_{j=0} \ dx, \qquad (A.1)$$

with $F_d(x)$ from Eq. (45). In the case of $j = 0$ both current densities j_p (holes) and j_n (electrons) are equal to zero. From Eqs. (21)-(22) we get

$$\frac{kT}{e} n_i'(x) + n_i(x) F_i(x) = 0, \qquad (A.2)$$

$$\frac{kT}{e} p_i'(x) - p_i(x) F_i(x) = 0, \qquad (A.3)$$

or, combining these expressions,

$$F_i(x) = \frac{kT}{2e} \frac{d}{dx} \ln\left[\frac{p_i(x)}{n_i(x)}\right], \qquad (A.4)$$

$$\frac{d}{dx} \ln[p_i(x) n_i(x)] = 0. \qquad (A.5)$$

Integrating in Eq. (A.1) with $F_i(x)$ from (A.4), we find

$$V_{bi} = l_{TF,s} F_s(-L/2) + l_{TF,c} F_c(L/2) + \frac{kT}{2e}\left\{\ln\left[\frac{p_i(L/2)}{n_i(L/2)}\right] - \ln\left[\frac{p_i(-L/2)}{n_i(-L/2)}\right]\right\}. \qquad (A.6)$$

Using the boundary conditions (32)-(35) with $j = 0$, we directly obtain

$$V_{bi} = \frac{1}{e}\left(\Delta_n^+ - \Delta_n^-\right). \qquad (A.7)$$

Accounting for Eq. (10), it follows immediately that

$$eV_{bi} = E_{A,c} - E_{A,s}. \qquad (A.8)$$

It should be also noted, that from Eq. (A.5) follows that the product $p_i(x) n_i(x)$ takes the constant value everywhere in the organic layer. To provide zero current in the absence of applied voltage and be consistent with Eqs. (26)-(27), we choose this constant equal to n_{int}^2.

* Electronic address: yampolsk@tgm.tu-darmstadt.de

[1] M.A. Lampert and A. Rose, Phys. Rev. **121**, 26 (1961).

[2] M.A. Lampert, Phys. Rev. **125**, 126 (1962).

[3] R. Baron, Phys. Rev. **137**, A272 (1965).

[4] R. Baron, J. Appl. Phys. **39**, 1435 (1968).

[5] M. Dawber, K.M. Rabe, and J.F. Scott, Rev. Mod. Phys. **77**, 1083 (2005).

[6] P.W.M. Blom and M.C.J.M. Vissenberg, Mater. Sci. Eng., R. **27**, 53 (2000).

[7] A.B. Walker, A. Kambili, and S.J. Martin, J. Phys.: Condens. Matter **14**, 9825 (2002).

[8] W.J.M. Naber, S. Faez, and W.G. van der Wiel, J. Phys. D: Appl. Phys. **40**, R205 (2007).

[9] F. So, B. Krummacher, M.K. Mathai, D. Poplavskyy, S.A. Choulis, and V.E. Choong, J. Appl. Phys. **102**, 091101 (2007).

[10] H. Antoniadis, J.N. Miller, D.B. Roitman, and I.H. Cambell, IEEE Trans. Electron Devices **44**, 1289 (1997).

[11] G.G. Malliaras, J.R. Salem, P.J. Brock, and C. Scott, Phys. Rev. B **58**, R13411 (1998).

[12] C. Giebeler, H. Antoniadis, D.D.C. Bradley, and Y. Shirota, J. Appl. Phys. **85**, 608 (1999).

[13] S. Shi, D. Ma, and J. Peng, Semicond. Sci. Technol. **22**, 249 (2007).

[14] M.A. Lampert and P. Mark, *Current injection in solids* (Academic Press, New York, 1970).

[15] P.W.M. Blom, M.J.M. de Jong, and J.J.M. Vleggaar, Appl. Phys. Lett. **68**, 3308 (1996).

[16] P.W.M. Blom, M.J.M. de Jong, and M.G. van Munster, Phys. Rev. B **55**, R656 (1997).

[17] F. Neumann, Yu.A. Genenko, R. Schmechel, and H. von Seggern, Synth. Met. **150**, 291 (2005).

[18] S.M. Sze, *Physics of Semiconductor Devices* (John Wiley & Sons, Inc., New York, 1969).

[19] V.I. Arkhipov, P. Heremans, E.V. Emelianova, and G.J. Adriaenssens, Appl. Phys. Lett. **79**, 4154 (2001).

[20] V.I. Arkhipov, H. von Seggern, and E.V. Emelianova, Appl. Phys. Lett. **83**, 5074 (2003).

[21] S.J. Martin, A.B. Walker, A.J. Campbell, and D.C. Bradley, J. Appl. Phys. **98**, 063709 (2005).

[22] Y. Preezant and N. Tessler, J. Appl. Phys. **93**, 2059 (2003).

[23] F. Neumann, Yu.A. Genenko, C. Melzer, and H. von Seggern, J. Appl. Phys. **100**, 084511 (2006).

[24] F. Neumann, Yu.A. Genenko, C. Melzer, S.V. Yampolskii, and H. von Seggern, Phys. Rev. B **75**, 205322 (2007).

[25] J.C. Scott, P.J. Brock, J.R. Salem, S. Ramos, G.M. Malliaras, S.A. Carter, and L. Bozano, Synth. Met. **111-112**, 289 (2000).

[26] B. Ruhstaller, S.A. Carter, S. Barth, H. Riel, W. Riess, and J.C. Scott, J. Appl. Phys. **89**, 4575 (2001).

[27] M. Pope and Ch.E. Swenberg, *Electronic Processes in Organic Crystals and Polymers* (Oxford University Press, Oxford, 1999).

[28] P. Langevin, Ann. Chem. Phys. **28**, 289 (1903).

[29] J. Shen and J. Yang, J. Appl. Phys. **83**, 7706 (1998).

[30] P.W.M. Blom, M.J.M. de Jong, and S. Breedijk, Appl. Phys. Lett. **71**, 930 (1997).

[31] P.W.M. Blom and M.J.M. de Jong, IEEE J. Sel. Top. Quantum Electron. **4**, 105 (1998).

[32] P.W.M. Blom and M.J.M. de Jong, Philips J. Res. **51**, 479 (1998).

[33] C.D.J. Blades and A.B. Walker, Synth. Met. **111-112**, 335 (2000).

[34] S.J. Martin, J.M. Lupton, I.D.W. Samuel, and A.B. Walker, J. Phys.: Condens. Matter **14**, 9925 (2002).

[35] G.G. Malliaras and J.C. Scott, J. Appl. Phys. **83**, 5399 (1998).

[36] G.G. Malliaras and J.C. Scott, J. Appl. Phys. **85**, 7426 (1999).

[37] E. Tutiš, M.N. Bussac, B. Masenelli, M. Carrard, and L. Zuppiroli, J. Appl. Phys. **89**, 430 (2001).

[38] R. Bel Hadj Tahar, T. Ban, Y. Ohya, and Y. Takahashi, J. Appl. Phys. **83**, 2631 (1998).

[39] N.D. Lang and W. Kohn, Phys. Rev. B **3**, 1215 (1971).

[40] L.D. Landau and E.M. Lifshitz, *Electrodynamics of Continuous Media* (Pergamon, Oxford, 1989).

[41] N.W. Ashcroft and N.D. Mermin, *Solid State Physics* (Thomson Learning, Inc., Florence, 1976).

[42] D. Mergel and Z. Qiao, J. Phys. D: Appl. Phys. **35**, 794 (2002).

[43] D. Mergel and Z. Qiao, J. Appl. Phys. **95**, 5608 (2004).

[44] H. Fujiwara and M. Kondo, Phys. Rev. B **71**, 075109 (2005).

[45] R.H. Parmenter and W. Ruppel, J. Appl. Phys. **30**, 1548 (1959).

[46] H. Ishii, K. Sugiyama, E. Ito, and K. Seki, Adv. Mater. (Weinheim, Ger.) **11**, 605 (1999).

[47] A. Kahn, N. Koch, and W. Gao, J. Polym. Sci. B—Polym. Phys. **41**, 2529 (2003).

[48] V.I. Arkhipov, E.V. Emelianova, Y.H. Tak, and H. Bässler, J. Appl. Phys. **84**, 848 (1998).

[49] A. Opitz, M. Bronner, and W. Brütting, J. Appl. Phys. **101**, 063709 (2007).

[50] D.M. Pai, J. Chem. Phys. **52**, 2285 (1970).

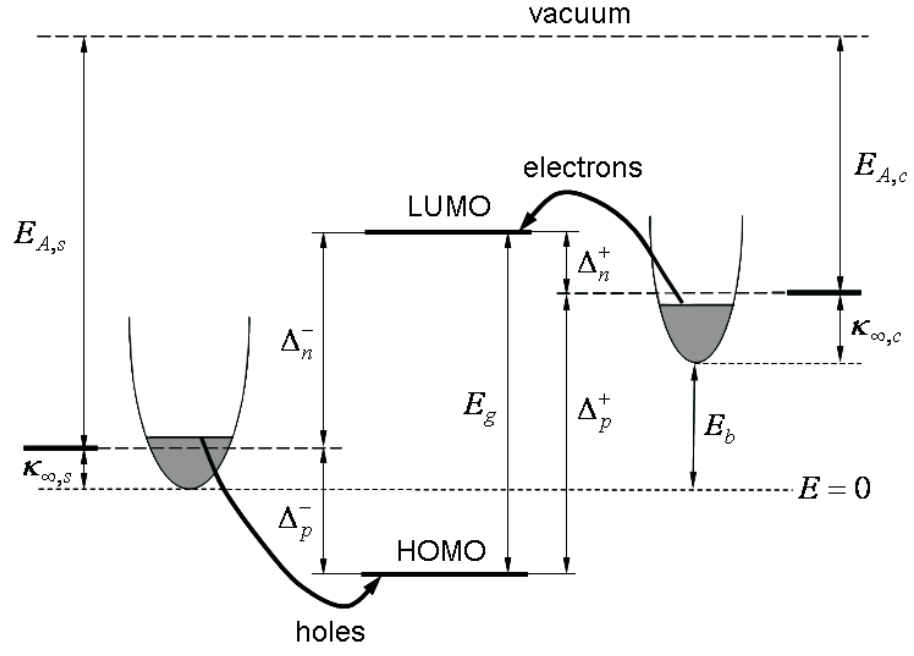[51] P.N. Murgatroyd, J. Phys. D: Appl. Phys. **3**, 151 (1970).

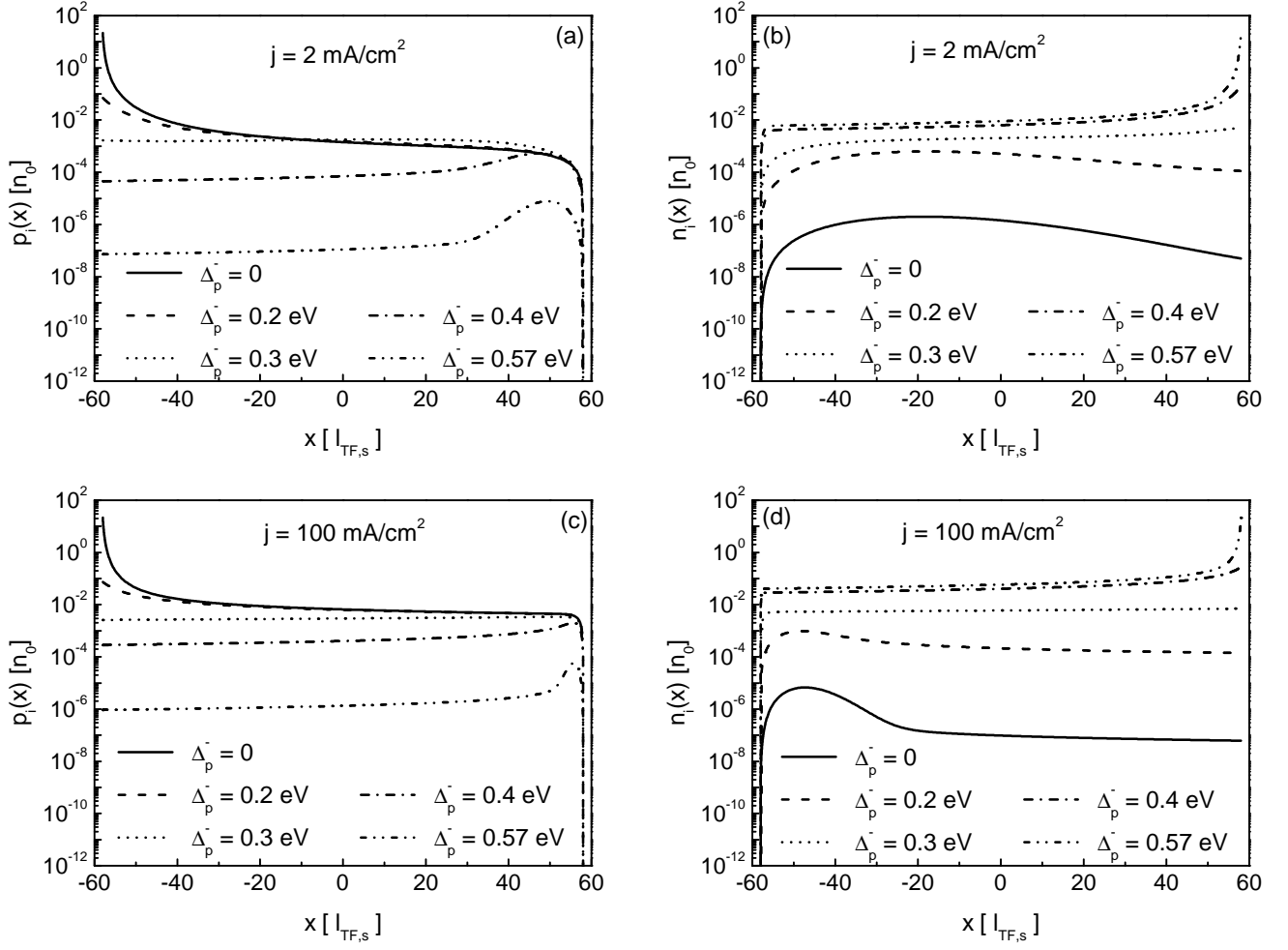FIG. 1: Schematic band diagram of the considered semiconductor/insulator/conductor structure.

FIG. 2: Spatial distributions of the charge-carrier densities, p_i and n_i, in units of $n_0 = \epsilon_i \epsilon_0 kT / e^2 l_{TF,s}^2$ for a system without recombination for different barrier heights Δ_p^- and a constant current density: [(a) and (b)] $j = 2$ mA/cm^2 and [(c) and (d)] $j = 100$ mA/cm^2.
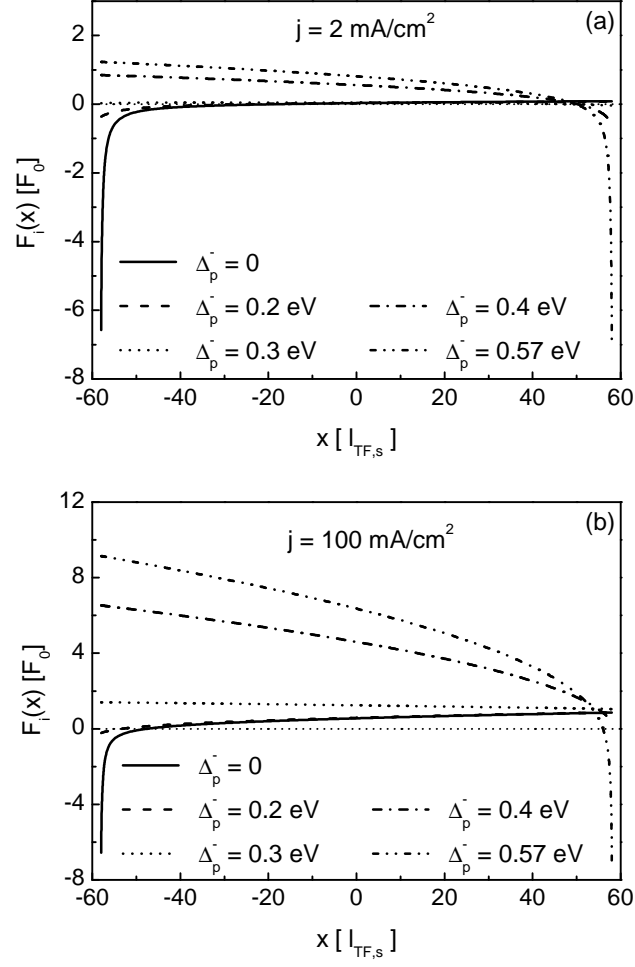
FIG. 3: Spatial distributions of the electric field F_i in units of $F_0 = kT/el_{TF,s}$ for a system without recombination for different barrier heights Δ_p^- and a constant current density: (a) $j = 2$ mA/cm^2 and (b) $j = 100$ mA/cm^2.

15
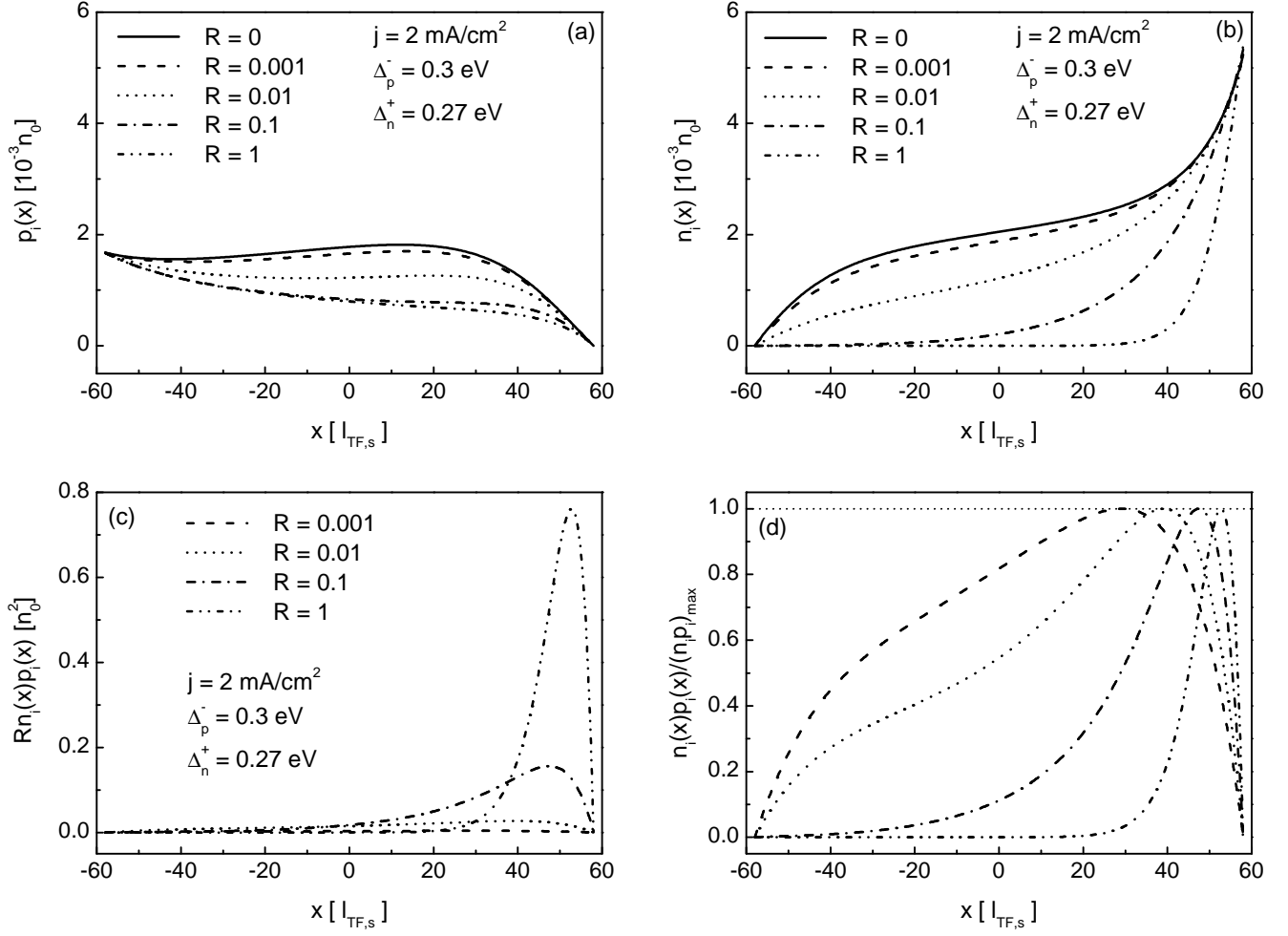
FIG. 4: Spatial distributions of (a) the hole density p_i, (b) the electron density n_i, (c) the recombination rate, and (d) the recombination zone $\sim n_i p_i$ for a system with the barrier height $\Delta_p^- = 0.3$ eV and the current density $j = 2$ mA/cm^2 for different values of the recombination parameter R. The carrier densities are measured in units of $n_0 = \epsilon_i \epsilon_0 kT/e^2 l_{TF,s}^2$. The product $n_i p_i$ in the part (d) is normalized on its maximum value.
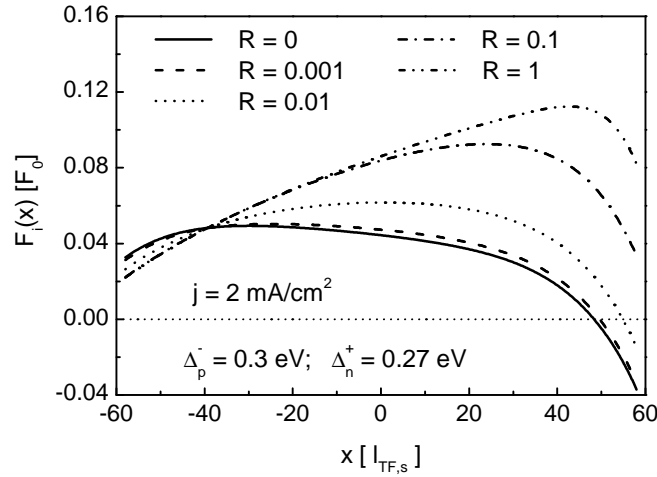
FIG. 5: Spatial distributions of the electric field F_i in units of $F_0 = kT/el_{TF,s}$ for a system with the barrier height $\Delta_p^- = 0.3$ eV and the current density $j = 2$ mA/cm^2 for different values of the recombination parameter R.
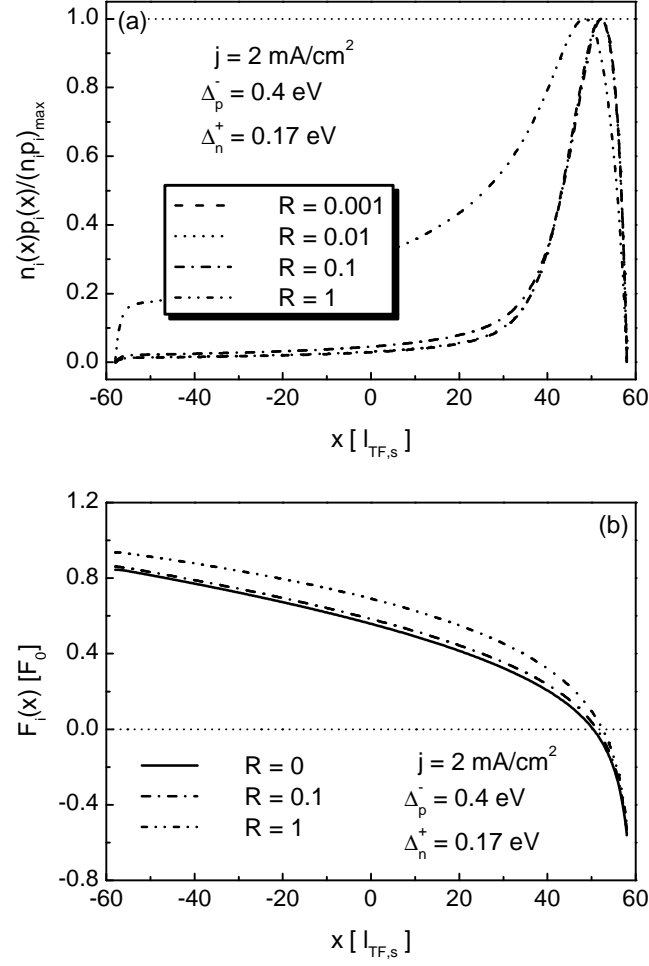
FIG. 6: Spatial distributions of (a) the recombination zone $\sim n_i p_i$ and (b) the electric field F_i for a system with the barrier height $\Delta_p^- = 0.4$ eV and the current density $j = 2$ mA/cm^2 for different values of recombination parameter R. The electric field is measured in units of $F_0 = kT/el_{TF,s}$. The product $n_i p_i$ is normalized on its maximum value.
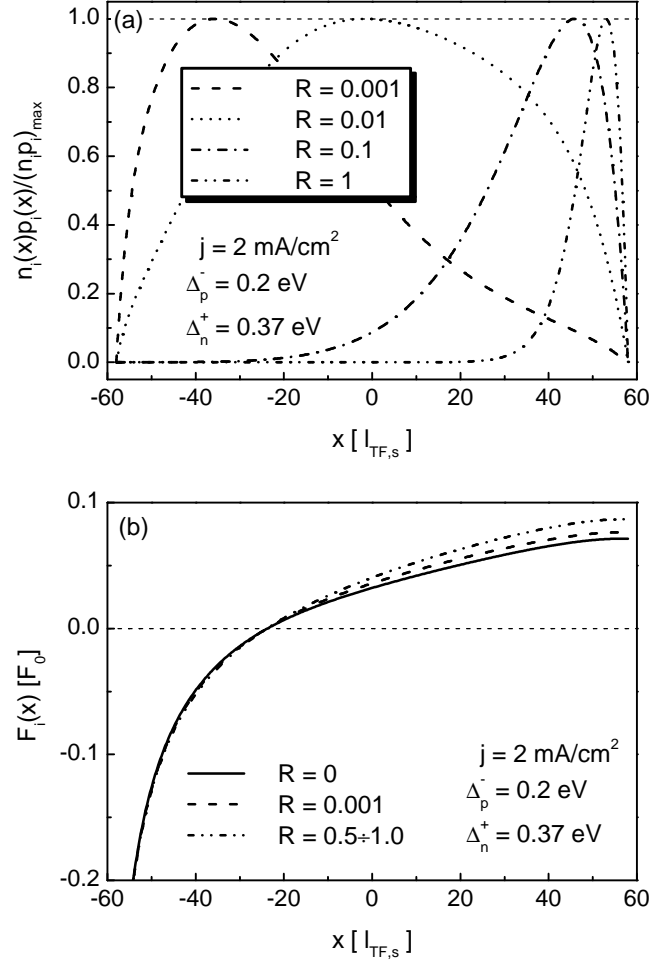
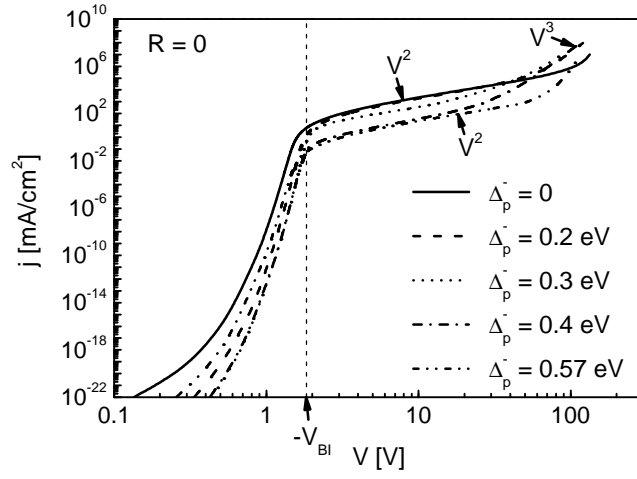FIG. 7: The same as in Fig. 6 but for the injection barrier height $\Delta_p^- = 0.2$ eV.

FIG. 8: *IV* characteristics of a system without recombination for barrier heights $\Delta_p^- = 0$, 0.2, 0.3, 0.4, and 0.57 eV.
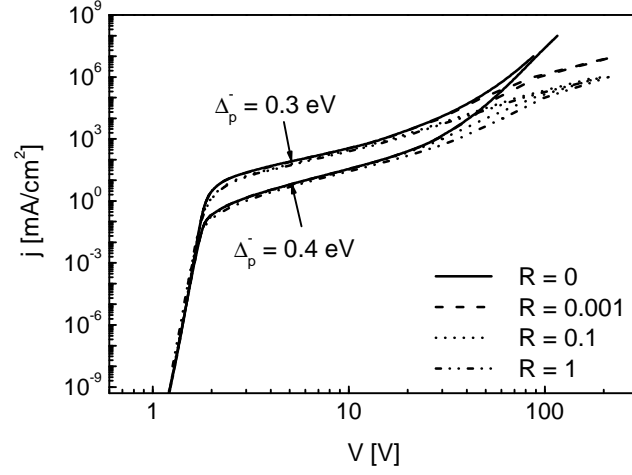
FIG. 9: *IV* characteristics of a system with barrier heights $\Delta_p^- = 0.3$ and 0.4 eV for different values of the recombination parameter R.
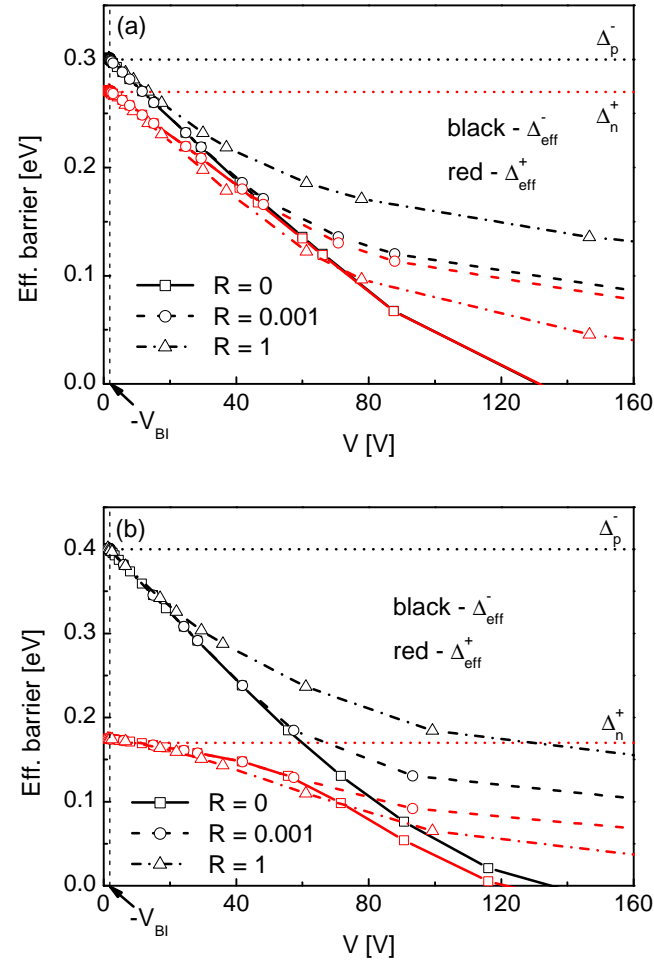
FIG. 10: Dependence of the effective injection barriers $\Delta_{\text{eff}}^{\pm}$ on the applied voltage for the barrier heights (a) $\Delta_p^- = 0.3$ eV and (b) 0.4 eV and for different values of the recombination parameter R.
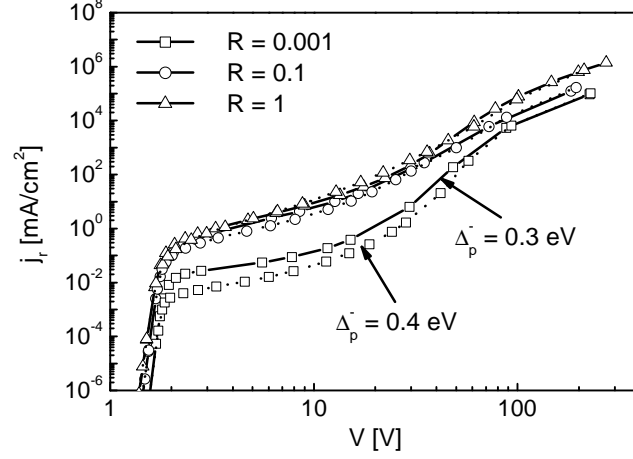
FIG. 11: Dependence of the recombination current density on the voltage V for a system with barrier heights $\Delta_p^- = 0.3$ eV (solid curves) and 0.4 eV (dotted curves) for different values of the recombination parameter R.
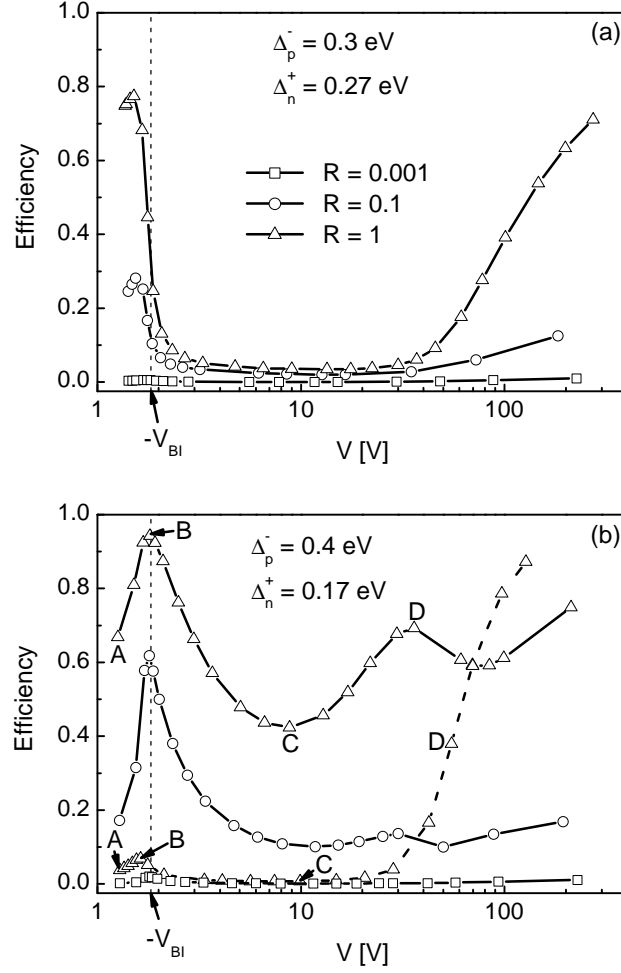

FIG. 12: Dependence of the recombination efficiency η_r on the voltage V for a system with barrier heights (a) $\Delta_p^- = 0.3$ eV and (b) 0.4 eV for different values of the recombination parameter: $R = 0.001$ (squares), $R = 0.1$ (circles) and $R = 1$ (triangles). The $\eta_r(V)$ dependence for $\Delta_p^- = 0.4$ eV, equal carrier mobilities $\mu_{p,i} = \mu_{n,i}$ and $R = 1$ is also shown by dashed curve.
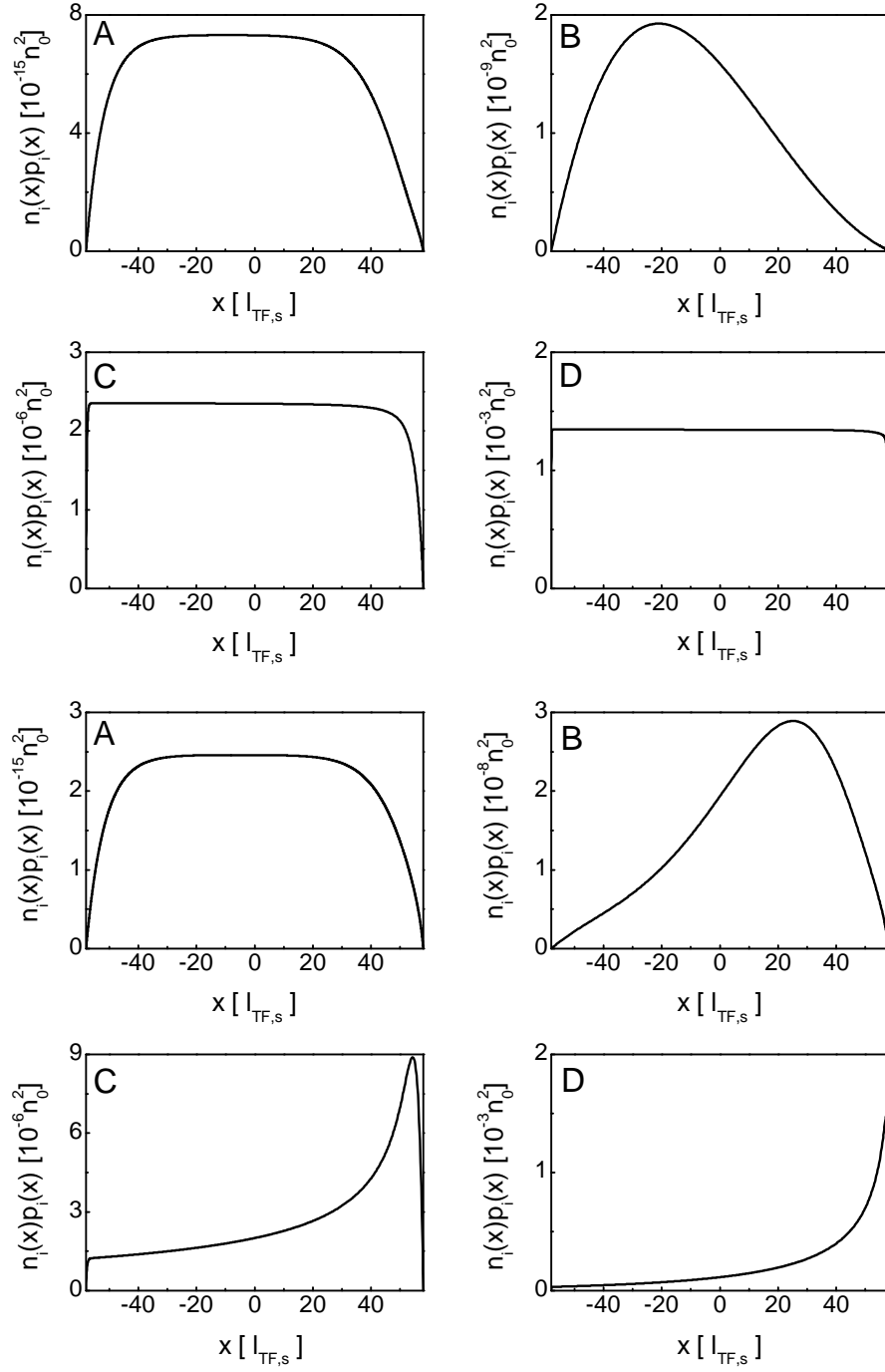
FIG. 13: Spatial distributions of the recombination zone $\sim n_i p_i$ at different voltage for a system with the barrier height $\Delta_p^- = 0.4$ eV, the recombination parameter $R = 1$ and the hole mobilities $\mu_{p,i} = \mu_{n,i}$ (upper four figures) and $\mu_{p,i} = 100\ \mu_{n,i}$ (bottom four figures) for the points of the $\eta_r\ (V)$ curves marked in Fig. 12,b by capital letters from A to D. The carrier densities are measured in units of $n_0 = \epsilon_i \epsilon_0 kT / e^2 l_{TF,s}^2$.
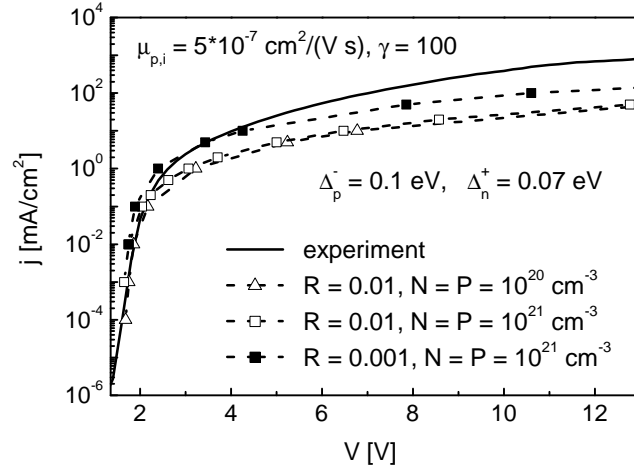
FIG. 14: Measured *IV* characteristic of ITO-PPV-Ca structure (solid curve) and its approximation with different values of the model parameters (dashed curves with symbols).
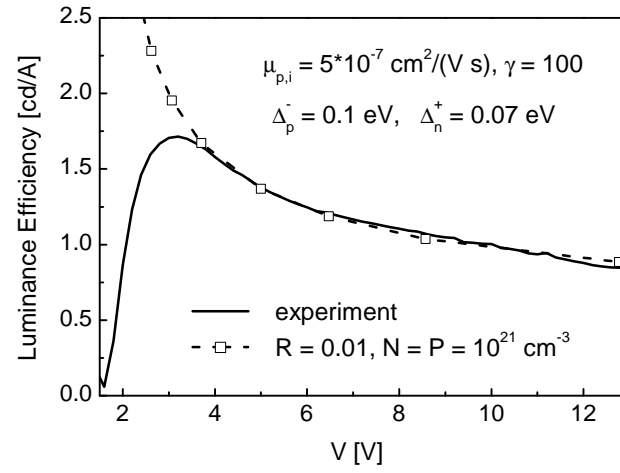

FIG. 15: Measured voltage dependence of the luminance efficiency of ITO-PPV-Ca structure (solid curve) and its fitting with the model parameters (dashed curve). The last dependence is shown in arbitrary units.